Microchimica Acta (2021) 188: 276
https://doi.org/10.1007/s00604-021-04926-7

ORIGINAL PAPER

Simultaneous electrochemical detection of guanine and adenine using reduced graphene oxide decorated with AuPt nanoclusters

Brennan Mao[1] · Lanting Qian[2] · Maduraiveeran Govindhan[1,3] · Zhonggang Liu[2,4] · Aicheng Chen[1,2]

Received: 24 April 2021 / Accepted: 4 July 2021 / Published online: 28 July 2021
© The Author(s), under exclusive licence to Springer-Verlag GmbH Austria, part of Springer Nature 2021

Abstract

A rapid and sensitive electrochemical sensing platform is reported based on bimetallic gold-platinum nanoclusters (AuPtNCs) dispersed on reduced graphene oxide (rGO) for the simultaneous detection of guanine and adenine using square wave voltammetry (SWV). The synthesis of AuPtNCs-rGO nanocomposite was achieved by a simultaneous reduction of graphene oxide (GO) and metal ions (Au^{3+} and Pt^{4+}) in an aqueous solution. The developed AuPtNCs-rGO electrochemical sensor with the optimized 50:50 bimetallic (Au:Pt) nanoclusters exhibited an outstanding electrocatalytic performance towards the simultaneous oxidation of guanine and adenine without the aid of any enzymes or mediators in physiological pH. The electrochemical sensor platform showed low detection limits of 60 nM and 100 nM ($S/N = 3$) for guanine and adenine, respectively, with high sensitivity and an extensive linear range from 1.0 μM to 0.2 mM for both guanine and adenine. The interference from the most common electrochemically active interferents, including ascorbic acid, uric acid, and dopamine, was almost negligible. The simultaneous sensing of guanine and adenine in denatured Salmon Sperm DNA sample was successfully achieved using the proposed platform, showing that the AuPtNCs-rGO nanocomposite could provide auspicious clinical diagnosis and biomedical applications.

Keywords Electrochemical sensing · Square wave voltammetry · Guanine · Adenine · Reduced graphene oxide · AuPt nanoclusters

Introduction

Deoxyribonucleic acid (DNA) and ribonucleic acid (RNA) are two biological molecules that play an important role in genetic information storage as well as in the protein synthesis. Purine bases, guanine (G) and adenine (A), are the building blocks of these biopolymers. These nitrogenous bases not only participate in storing genetic information, but also are involved in many biological processes such as energy transduction, cell signaling cascades, and regulation of metabolic enzyme activities [1]. Abnormality in their concentrations in human systems is suggested to be indicative of cancers, AIDS, Parkinson's diseases, renal diseases, and many other diseases that affect the metabolic pathways of these molecules [2–4]. Thus, it is of great significance in establishing a rapid and sensitive analytical method to determine and quantify the concentration of guanine and adenine for clinical diagnosis purpose.

To date, various methods have been developed for the analysis of guanine and adenine, such as chemiluminescence, surface enhanced Raman spectroscopy (SERS), high-performance liquid chromatography (HPLC), and electrophoresis [5–8]. It was reported that these methods were capable of achieving high sensitivity and selectivity. However, these techniques may suffer from the high costs, sophisticated instruments, portability, and complicated sample preparation procedures. As an alternative, electrochemical sensors with the advantages of simplicity, rapidity, and

✉ Aicheng Chen
aicheng@uoguelph.ca

1 Department of Chemistry, Lakehead University, 955 Oliver Road, Thunder Bay, ON P7B 5E1, Canada

2 Electrochemical Technology Centre, Department of Chemistry, University of Guelph, 50 Stone Road East, Guelph, ON N1G 2W1, Canada

3 Present address: Department of Chemistry, SRM Institute of Science and Technology, SRM Nagar, Kattankulathur, Chennai, Tamil Nadu 603 203, India

4 Present address: Institutes of Physical Science and Information Technology, Anhui University, 111 Jiulong Road, Hefei, Anhui, People's Republic of China

cost-effectiveness have emerged as a promising platform for the detection of guanine and adenine [9]. In the past decades, much effort involved of the electrochemical techniques and the various nanomaterials has been made on the oxidation of guanine and adenine. Specifically, square wave voltammetry (SWV) has shown to be a promising technique because of its high sensitivity in the detection of biomolecules, which is derived from the pulses applied to the staircase potential waveform during the sampling time [10, 11].

The rapid development of novel nanomaterials has provided great opportunities in designing promising electrochemical sensors [12–14]. Suitable nanomaterial-based electrochemical sensors may significantly improve electron transfer kinetics, sensitivity, selectivity, and reproducibility towards the detection of guanine and adenine compared with the unmodified electrode [15, 16]. Nanomaterials such as cobalt hexacyanoferrate film, PbO_2-carbon nanotube-ionic liquid composite, and dopamine-melanin nanosphere-polyaniline have been reported on the detection of guanine and adenine [17–19]. Notably, carbon-based nanomaterials have been widely used as supporting materials for numerous electrochemical sensor applications. Among the carbon-based materials, graphene, a two-dimensional layer of sp^2 hybridized carbon atoms packed in a honeycomb lattice, has been widely employed due to its large surface area and high electrical conductivity [20–22]. The aforementioned properties make graphene a great nanomaterial for enhancing the sensitivity of the electrode, and as a platform for the deposition of additional nanomaterials, which may induce synergistic effects. For examples, the over-oxidized polypyrrole/graphene nanocomposite, Fe_3O_4 nanoparticle–graphene oxide nanocomposite, and the TiO_2 nanofiber on graphene oxide nanosheets demonstrated the great sensitivities towards the electrochemical oxidation of guanine and adenine [22–24]. Further studies on the anodized epitaxial graphene electrode or the boron-doped and nitrogen-doped graphene film showed the enhanced electrocatalytic activity towards the detection of guanine and adenine [25, 26].

Noble metal nanoclusters represent an emerging nanomaterial class for biomedical applications owing to their fascinating optical, electrical, and physical properties that are vastly different from their larger counterparts [27–30]. Due to its unique optical and chemical properties, gold nanoclusters (AuNCs) have attracted great attentions and are employed in many applications [31, 32]. Many synthetic strategies have been proposed for the preparation of AuNCs. A common approach is to utilize polymers or biomolecule as a template for the gold nanoclusters to grow on, and the other method relies on self-assembled thiolate layer to offer protection for the gold atoms [33]. These approaches have been widely adopted for the synthesis of PtNCs and AgNCs [34–37]. Among all the solution-based synthetic strategies, the bottom-up approach has been extensively studied by chemically reducing Au^{3+} in the presence of thiol-stabilizing/capping agent [37]. Although Au or Pt nanoparticles in combination with graphene have been widely reported for electrochemical detection of many biomolecules and metallic ions [38–41], the application of AuPt nanoclusters/graphene nanocomposite has not been reported for the electrochemical detection of guanine and adenine.

In the present study, we have synthesized the gold-platinum nanoclusters/reduced graphene oxide (AuPtNCs-rGO) nanocomposites and explored their application for the sensitive electrochemical detection of guanine and adenine in neutral pH. The simultaneous guanine and adenine electrochemical sensing platform was established by integrating the AuPtNCs and rGO sheets, where a simple bottom-up approach was developed for the synthesis of AuPtNCs-rGO nanocomposite. SWV was employed to investigate the simultaneous electrochemical detection of guanine and adenine at the AuPtNCs-rGO nanocomposite. The nanocomposite demonstrated a high electrocatalytic activity towards the oxidation of guanine and adenine in comparison with the bare glassy carbon electrode (GCE), AuNCs-rGO/GCE and PtNCs-rGO/GCE. The molar ratio of Au:Pt in the nanocomposite was optimized based on the peak current densities as well as the oxidation potentials of guanine and adenine. The developed AuPtNCs-rGO nanocomposite exhibited an excellent stability and selectivity and was further employed for the detection of the guanine and adenine in salmon sperm ssDNA sample.

Experimental section

Materials and reagents Adenine, guanine, and salmon sperm dsDNA were purchased from Sigma-Aldrich. Gold(III) chloride trihydrate ($AuCl_3·6H_2O$), $H_2PtCl_6·6H_2O$, graphene oxide, $NaBH_4$, NaH_2PO_4, Na_2HPO_4, Nafion (10 wt% in water) solution, and all other chemicals were obtained from Sigma-Aldrich. All analytical grade reagents were used as received without any further purification. The stock solutions of adenine and guanine (20 mM) were prepared by dissolving in 0.1 M NaOH solution and refrigerated at 4 °C; and the standard solutions were prepared from these stock solutions. The phosphate buffer (PB, 0.1 M, pH 7.2) solution prepared from NaH_2PO_4 and Na_2HPO_4 was used as the supporting electrolyte throughout the experiments. All solutions were prepared using pure water (18.2 MΩ·cm) obtained by NANOpure® Diamond™ UV ultrapure water purification system.

Characterization and electrochemical measurements The surface morphology of the nanocomposite was investigated using scanning electron microscopy (Hitachi SU-70 SEM) with an energy-dispersive X-ray spectrometer and transmission electron microscopy (JEOL 2010F-TEM). XPS spectra were obtained with a Thermo Scientific Kα XPS system, where the size of the X-ray spot was 400 mm with an Al Kα monochromatic source. For electrochemical measurements, cyclic voltammetry and SWV were performed using a CHI 660D electrochemical workstation (CHI instrument, USA). A three-electrode, single-compartment cell was used. The unmodified or modified glassy carbon electrode (GCE) with a surface area of 0.07 cm^2 was used as the working electrode, silver/silver chloride electrode (Ag/AgCl, 1 M KCl) as the reference electrode, and a platinum coil as the counter electrode. All the current densities reported in this study were calculated based on the geometric surface area of the GCE (0.07 cm^2). All the SWV measurements were conducted using the following parameters: increment E = 4 mV; amplitude = 25 mV; frequency f = 15 Hz; quiet time t = 2 s. All potentials were measured and reported vs. Ag/AgCl (1 M KCl), and all electrochemical measurements were performed under room temperature (20 ± 2 °C).

Preparation of AuPtNCs-rGO nanocomposites The synthesis strategy applied in this work was slightly modified from previously reported method for red-emitting gold quantum clusters [33]. For preparing the $Au_{50}Pt_{50}$NCs-rGO, 17 μL of 150 mM $AuCl_3{\cdot}6H_2O$ and 17 μL of 150 mM $H_2PtCl_6{\cdot}6H_2O$ stock solutions were dissolved in 2.736 mL water in a 10-mL glass vial. Similarly, the Au:Pt of 25:75 was prepared using 17 μL of 75 mM $AuCl_3{\cdot}6H_2O$ and 17 μL of 225 mM $H_2PtCl_6{\cdot}6H_2O$, while the Au:Pt of 75:25 was prepared using 17 μL of 225 mM $AuCl_3{\cdot}6H_2O$ and 17 μL of 75 mM $H_2PtCl_6{\cdot}6H_2O$. Subsequently, 8.82 mg of glutathione and 1.01 mL graphene oxide (4 mg mL^{-1}) were added to the solution under stirring and allowed to cool in an ice water bath. Then, 0.305 mL of the freshly prepared ice-cold $NaBH_4$ solution (2.0 mg mL^{-1}) was slowly added to the mixture and well-stirred for 40 min in an ice bath.

Preparation of salmon sperm ssDNA sample Salmon sperm dsDNA was thermally denatured using previously reported method [23]. The DNA sample (20 mg) was dissolved in 8 mL water and heated in an oil bath at 100 °C for 10 min, and immediately cooled in an ice-water bath for another 10 min to generate the ssDNA sample for analytical application.

Fabrication of the electrochemical sensor Prior to any modification, the GCE was first polished with alumina powder (0.05 μm) on chamois leather pad, washed thoroughly with doubly distilled water, followed by an ultrasonic bath in doubly distilled water for 3 min, and air-dried before use. The GCE was then pretreated by electrochemical oxidation, initially at 1.75 V for 300 s, followed by electrochemical reduction at −1.75 V for 300 s in 0.1 M PBS (pH 7.2) solution. The pretreated GCE was then scanned between 0 and 0.8 V at a scan rate of 100 mV s^{-1} until a stable cyclic voltammetric curve was achieved. Prior to the modification, the nanocomposite was stirred vigorously for 10 min to obtain a homogenous solution, and 10 μL of the solution containing Nafion (2 wt%) was then casted on the surface of the pretreated GCE and allowed to air-dry.

Results and discussion

Surface characterization of the AuPtNCs-rGO nanocomposite The surface morphology of the as-synthesized AuPtNCs-rGO nanocomposite was characterized by TEM. Figure 1A shows the low-resolution TEM image of the formed AuPtNCs-rGO nanocomposite. The ultrathin rGO nanosheets can be observed in the TEM image (Fig. 1A), which may provide the solid platform for the formation of AuPtNCs. Figure 1B displays the high-resolution TEM image of the AuPtNCs-rGO nanocomposite, where the presence of gold and platinum was confirmed using EDX (Fig. S1). It was apparent that the AuPtNCs presented are spherical structures and are uniformly dispersed in rGO. The homogenous nanoclusters demonstrated that the Au and Pt were alloyed, and the average particle size of the AuPtNCs was determined to be ~1.2 nm. Based on the TEM results, the well-dispersed characteristic and small size of AuPtNCs increase the electrochemically active surface area and may then enhance the electron transfer for the oxidation of guanine and adenine.

In order to characterize the valence states and surface composition of the nanocomposite, XPS was applied to analyze the AuPtNCs-rGO with various AuPt compositions. Based on the survey spectra of the formed nanocomposites, the ratios of Au:Pt were confirmed and tabulated in Table S1. The Au 4f spectra (Fig. 2A) and Pt 4f spectra (Fig. 2B) of the nanocomposites were deconvoluted to determine their oxidation state. In the case of Au 4f, the peaks for Au(0) and Au(I) were observed, which was attributed to the tendency of the thiolated clusters to be reduced in a stepwise fashion, from Au(III) to Au(I), before reaching Au(0) [42]. Similarly, in the Pt 4f spectrum (Fig. 2B), the two oxidation states for Pt were Pt(0) and Pt(II), as the Pt(IV) precursor was also reduced in a stepwise fashion [43]. The binding energies of the Au(0) and Pt(0) states were tabulated for each composition in Table S1. It can be observed that the binding energy of the Au(0) state was decreased with the introduction of Pt into the nanocomposite. The lowest binding energies of both the Au(0) and Pt (0) were achieved as the molar ratio of Au:Pt was 50:50, while the binding energies were increased with further increasing the Pt content. As reported, the Au-Pt alloying could result in a slight decrease in the binding energy of the Pt and Au [43]. Thus, the result suggested the formation of alloys of Au and Pt as a nanocomposite. The synergistic effect of the bimetallic AuPt alloy with the AuPt molar ratio of 50:50 could be

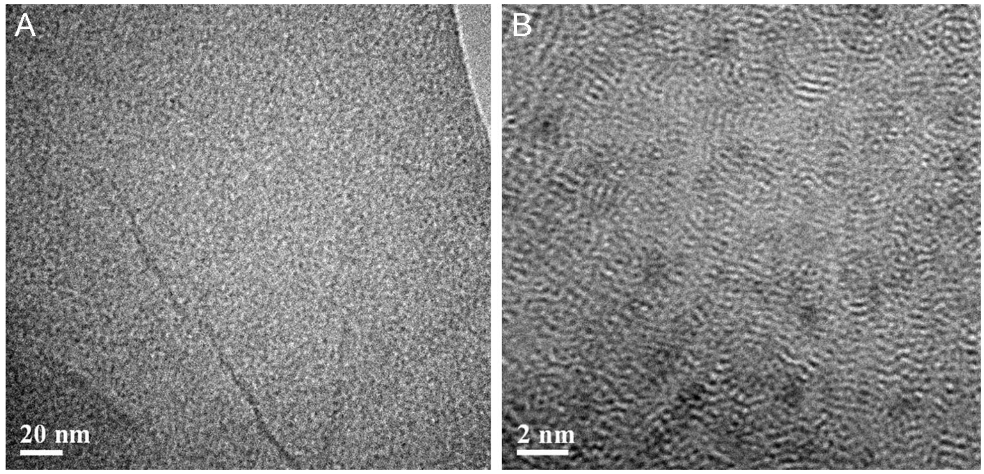

Fig. 1 (A) Low-resolution and (B) high-resolution TEM image of $Au_{50}Pt_{50}$NCs-rGO nanocomposite

significantly maximized and improved, which could potentially result in a lowered oxidation potential and an increased peak current density of guanine and adenine oxidation. Figure 2C shows the C 1s spectra of the AuPtNCs-rGO nanocomposites. Based on the binding energy of the individual peaks, it can be identified that there were various types of carbon bonding: sp^2 hybridized carbon, C–O, C=O, and O–C=O based on the literature values [44]. The characteristic peaks with binding energies at 284.68, 286.31, 287.98, and 288.74 eV can be assigned to sp^2 carbon, C–O, C=O, and O–C=O, respectively. And it can be concluded that more than 50% of the carbons were converted to sp^2 hybridized carbon (red curve) in the nanocomposite, showing that graphene oxide has been successfully reduced using a chemical reduction method, and provided the platform for anchoring the bimetallic nanoclusters.

Optimization of the Au:Pt ratio in the AuPtNCs-rGO nanocomposites For comparison, the SWV responses of 50 μM guanine and adenine in 0.1 M PB solution (pH 7.2) at the GCE and rGO/GCE are presented in Fig. S-2, where the dashed curves were recorded in the absence of guanine and adenine. The peak potential and peak current for guanine oxidation at the GCE were 0.83 V and 7.03 μA cm^{-2}, while for adenine they were 1.17 V and 11.84 μA cm^{-2}, respectively. The rGO/GCE exhibited a much lower peak potential for guanine (0.68 V) and adenine (0.99 V) and a much higher peak current for guanine (13.63 μA cm^{-2}) and adenine oxidation (33.20 μA cm^{-2}), showing that the modification of the GCE with the rGO enhanced the electrochemical oxidation of guanine and adenine. In order to study the effect of the Au:Pt ratio in AuPtNCs-rGO on the electrochemical performance, we further investigated the electrochemical oxidation of guanine and adenine at the AuPtNCs-rGO with different Au and Pt molar ratios. Figure 3A shows the SWV responses of 50 μM guanine and adenine at the AuPtNCs-rGO/GCE with different AuPt molar ratios in 0.1 M PB solution (pH 7.2), where the dashed lines represented as the SWV responses in the absence of guanine and adenine. There was no obvious change on the SWV curves by varying the AuPt molar ratios. The corresponding current densities (j_{pa}) and the oxidation potentials for 50 μM guanine and adenine were collected

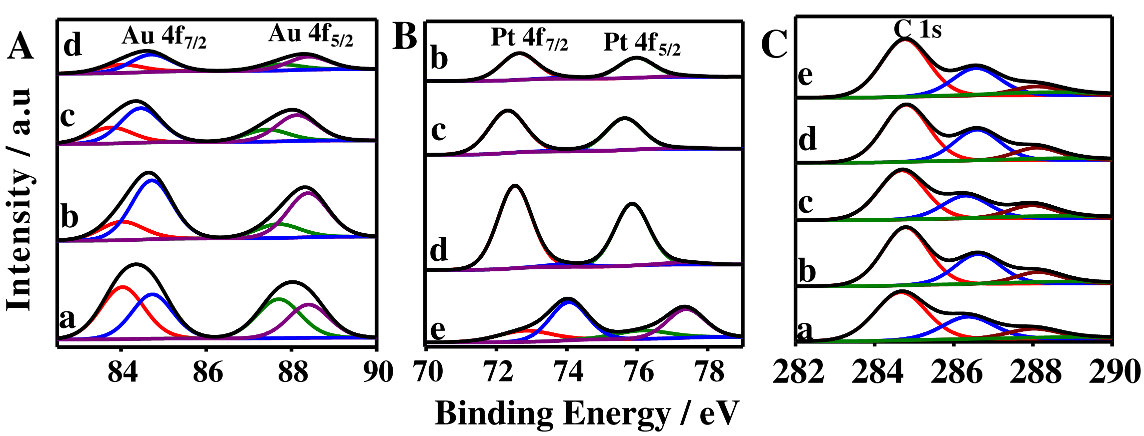

Fig. 2 High-resolution of XPS spectra of (A) Au 4f, (B) Pt 4f, and (C) C 1s in AuPtNCs-rGO nanocomposite with the Au:Pt molar ratio of (a) 100:0, (b) 75:25, (c) 50:50, (d) 25:75, and (e) 0:100

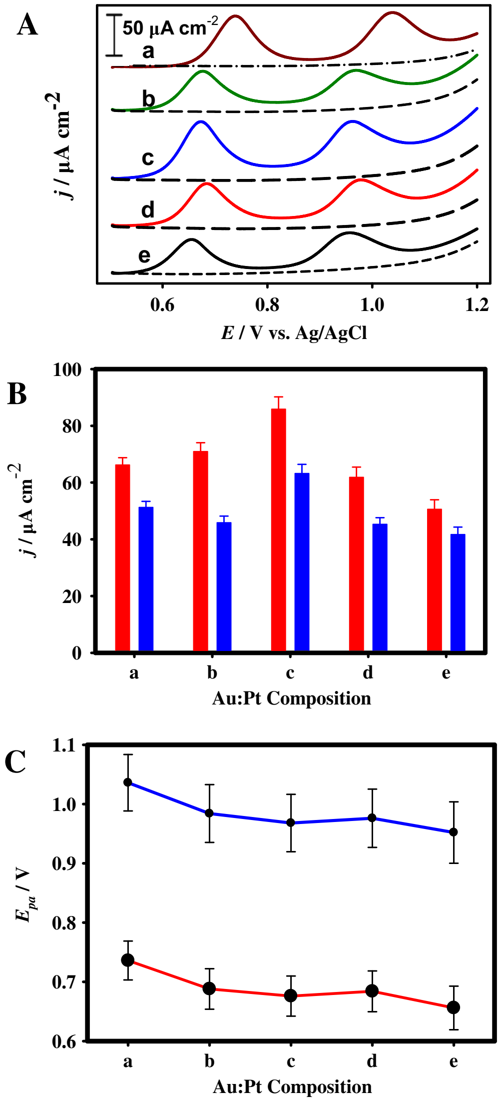

Fig. 3 (A) SWV responses of 50 µM guanine and adenine at AuPtNCs-rGO/GCE with the Au:Pt molar ratio of (a) 100:0, (b) 75:25, (c) 50:50, (d) 25:75, and (e) 0:100. Dependence of the peak current densities (B) and the corresponding peak potentials (C) of 50 µM guanine and adenine at the AuPt-rGO/GCE with different AuPt molar ratios. Error bars represent the standard deviation over three consecutive measurements

and presented in Fig. 3B and C. As shown in Fig. 3B, the current densities of guanine and adenine were increased as the Au/Pt molar ratio was decreased from 100:0 to 50:50, while the responses were decreased with the further decrease in the percent of Au, revealing that the much higher SWV responses can be achieved with the Au/Pt ratio of 50:50. As the AuPt molar ratio was changed from 100:0 to 0:100, the oxidation potentials were decreased from 0.736 to 0.656 V for guanine, and from 1.036 to 0.952 V for adenine, respectively (Fig. 3C). In comparison with that of the AuNCs-rGO/GCE, the oxidation peak potentials of guanine and adenine at the $Au_{50}Pt_{50}$NCs-rGO were positively shifted 60 mV and 68 mV, respectively. As reported, the redox potential suggested the thermodynamic information on the electrochemical reactions. This result indicated that the oxidation of guanine and adenine at the AuNCs-rGO/GCE was a kinetic limitation process [45]. The introduction of Pt and the formation of bimetallic AuPt can modify the surface electronic structure, and greatly increase the SWV responses resulting from the efficient synergy effect [46]. The aforementioned results suggested that AuPtNCs-rGO with the Au:Pt ratio of 50:50 was selected as the ideal composition in the nanocomposite for the further detection of guanine and adenine.

Effect of the scan rate on the oxidation of guanine and adenine Figure S3A shows the effect of scan rate on the electrochemical oxidation of guanine and adenine at the $Au_{50}Pt_{50}$NCs-rGO/GCE, which was investigated with 50 µM guanine and adenine in 0.1 M PBS solution (pH 7.2) using CV technique. The scan rate was varied from 10 to 125 mV s^{-1}. As seen in Fig. S3A, the oxidation peak current densities of guanine and adenine were increased linearly at the $Au_{50}Pt_{50}$NCs-rGO/GCE as the scan rate increases. Figure S3FB displays the plot of current densities against the square root of the scan rate. The linear relationships for guanine and adenine were expressed as j_{pa} (µA cm^{-2}) = $6.90\upsilon^{1/2}$–10.7 (R^2 = 0.98) and j_{pa} (µA cm^{-2}) =$4.88\upsilon^{1/2}$–8.87 (R^2 = 0.99), respectively. This linear relationship demonstrated that the electrochemical oxidation of guanine and adenine on the surface of $Au_{50}Pt_{50}$NCs-rGO/GCE was a diffusion-controlled process.

Simultaneous detection of guanine and adenine The simultaneous detection of guanine and adenine was investigated at the $Au_{50}Pt_{50}$NC-rGO/GCE using the SWV technique scanning from 0.5 to 1.1 V vs Ag/AgCl (1 M KCl). The concentrations of guanine and adenine were changed simultaneously from 1.0 µM to 0.2 mM in 0.1 M PB (pH 7.2) solution. As shown in Fig. 4A, two distinct peaks can be observed at 0.670 and 0.970 V corresponding to the electrochemical oxidation of guanine and adenine, respectively. And the two anodic peaks increased progressively with the addition of the two analytes. Based on the peak current densities of guanine and adenine, the calibration curves are plotted in Fig. 4B and C, respectively, which demonstrated that the linear response of guanine and adenine can be achieved as the concentration increased. As shown in Fig. 4B and C, two dynamic linear ranges of 1.0 µM–20 µM and 20 µM–0.20 mM were obtained for both guanine and adenine. The sensitivities of the detection of guanine were calculated to be 1.80 µA μM^{-1} cm^{-2} (R^2 = 0.99) and 0.50 µA μM^{-1} cm^{-2} (R^2 = 0.99), respectively, while the obtained sensitivities for adenine detection were 1.56 µA μM^{-1} cm^{-2} (R^2 = 0.99) and 0.52 µA μM^{-1} cm^{-2} (R^2 = 0.98), respectively. It can be observed that the high sensitivity was achieved for both guanine and adenine at the low concentration and the low sensitivity was obtained for the high concentration. This result suggested that more oxidized products might be adsorbed on the surface of the electrode, which may hinder the accessibility of the active sites, resulting in a lower sensitivity. Furthermore, the detection limits were estimated to be 60 nM and 100 nM for guanine and adenine, respectively, based on the equation of 3σ/s, where "σ" represents the standard deviation of the blank and s is the slope of the calibration curve.

Besides, we studied the simultaneous detection of guanine and adenine at the AuNCs-rGO/GCE under the same conditions. Figure S4 shows the SWV responses towards guanine and adenine at the AuNCs-rGO/GCE measured by simultaneously changing the concentrations of guanine and adenine from 1.0 μM to 0.2 mM. As shown in Fig. S4A, a couple of distinct peaks at 0.72 V and 1.01 V were observed which corresponded to the oxidation of guanine and adenine, respectively. The anodic current densities increased with the increasing concentration of guanine and adenine. Figure S4B and S4C display the calibration plots for the sensing of guanine and adenine, where the anodic current density increased linearly for both guanine and adenine at the AuNCs-rGO/GCE. Two dynamic linear ranges of 1.0 μM–20.0 μM and 20.0 μM–0.2 mM were obtained for both guanine and adenine. The obtained sensitivities were 1.42 μA μM^{-1} (R^2 = 0.99) and 0.38 μA μM^{-1} (R^2 = 0.99) for guanine; the sensitivities for adenine detection were 1.55 μA μM^{-1} (R^2 = 0.98) and 0.44 μA μM^{-1} (R^2 = 0.98). The detection limits were calculated to be 290 nM and 110 nM for the sensing of guanine and adenine, respectively.

Since it has been reported that Pt-graphene nanocomposite was not able to detect adenine and guanine at the low concentration that covered the physiological concentration [47], we investigated the simultaneous detection of guanine and adenine in different concentrations at the PtNCs-rGO nanocomposite, where the guanine and adenine were added from 2.5 to 200 μM (Fig. S5A in supporting information). Within the tested concentration, the current responses of guanine and adenine were not observed until 10 μM and 2.5 μM, respectively. As demonstrated in Fig. S5B and S5C, the calibration curves for guanine and adenine at low and high concentration were j_{pa} (μA cm^{-2}) = 0.917c_g − 6.78 (R^2 = 0.97) and j_{pa} (μA cm^{-2}) = 0.200c_g + 39.9 (R^2 = 0.99), and j_{pa} (μA cm^{-2}) = 0.932c_a + 0.193 (R^2 = 0.97) and j_{pa} (μA cm^{-2}) = 0.254c_a + 23.3 (R^2 = 0.98), respectively. Based on the calibration curve, the sensitivities were found to be 0.917 μA μM^{-1} cm^{-2} and 0.200 μA μM^{-1} cm^{-2} for guanine, and 0.932 μA μM^{-1} cm^{-2} and 0.254 μA μM^{-1} cm^{-2} for adenine, respectively. The corresponding detection limits of guanine and adenine were calculated to be 1.5 μM and 0.8 μM (3σ/s). The detection limit of adenine was not able to cover the physiological concentration, making the PtNCs-rGO nanocomposite impractical. In comparison with the electrochemical performance of AuNCs-rGO/GCE and PtNCs-rGO/GCE, the

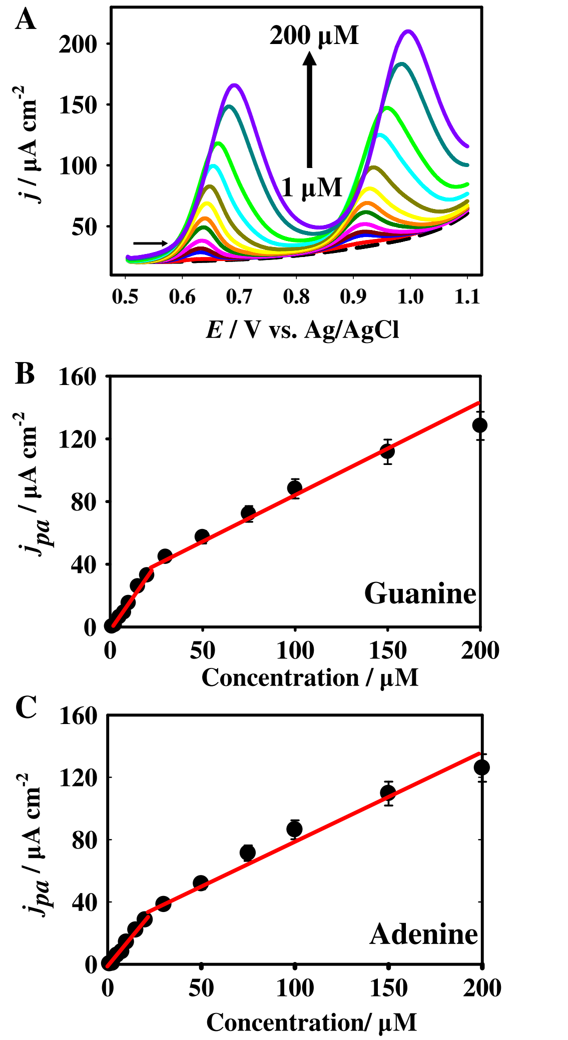

Fig. 4 (A) SWV responses of guanine and adenine oxidation at various concentrations and the corresponding calibration curves for (B) guanine and (C) adenine at the $Au_{50}Pt_{50}$NCs-rGO/GCE

$Au_{50}Pt_{50}$NC-rGO/GCE showed the much higher sensitivity and a lower detection limit at both lower and higher concentration range, demonstrating the enhancement in sensitivity using the bimetallic nanoclusters. We further compared the experimental results with those published in the recent literatures. As shown in Table S-2, the $Au_{50}Pt_{50}$NCs-rGO/GCE exhibited a lower detection limit and a wider linear range for the detection of both guanine and adenine over the recent studies reported in the literature, demonstrating the excellent electrochemical performance of the proposed $Au_{50}Pt_{50}$NCs-rGO nanocomposite.

Selectivity and stability measurements The selectivity of the $Au_{50}Pt_{50}$NCs-rGO/GCE towards the detection of guanine and adenine was evaluated in the presence of multiple coexisting compounds. Figure 5A shows the SWV

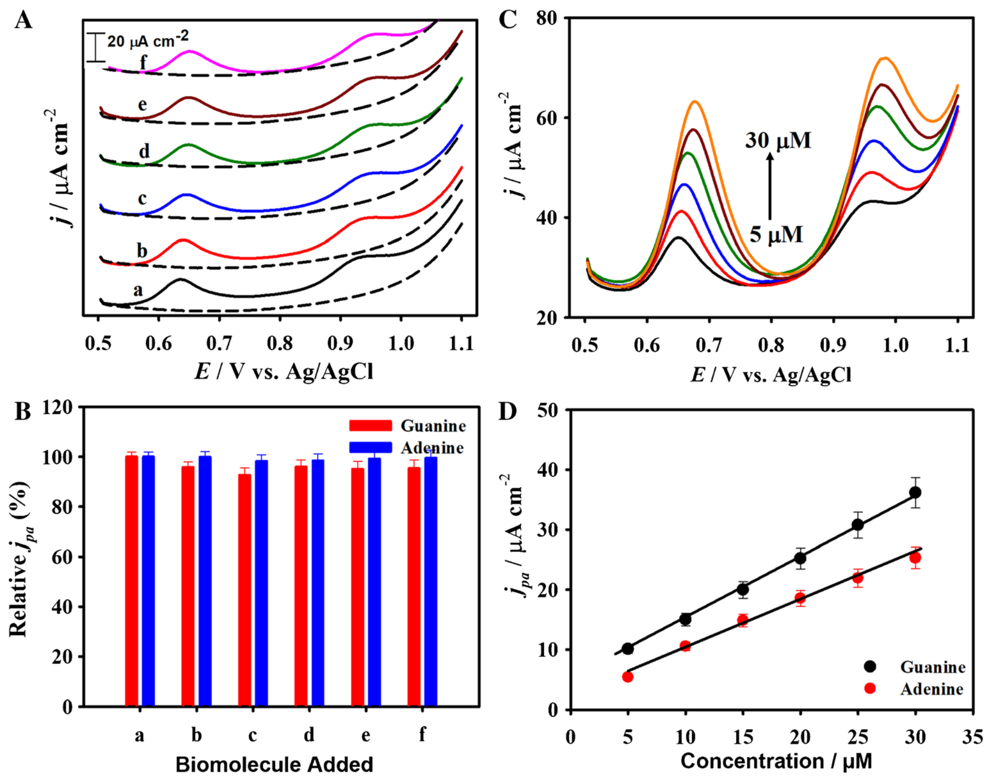

Fig. 5 (A) SWV curves at the $Au_{50}Pt_{50}$NCs-rGO/GCE after sequential addition of (a) guanine and adenine, (b) dopamine (DA), (c) glucose (Glu), (d) uric acid (UA), (e) cysteine (Cys), and (f) ascorbic acid (AA). Each concentration is 5.0 μM. (B) The change in the current densities of guanine and adenine in the absence and in the presence of the interferents. (C) SWV responses of guanine and adenine with different concentrations in the presence of the interferents and (D) the corresponding calibration curves of guanine and adenine

responses towards 5.0 μM guanine and adenine at the $Au_{50}Pt_{50}$NCs-rGO/GCE in the presence of 5.0 μM of dopamine (DA), glucose (Glu), uric acid (UA), cysteine (Cys), and ascorbic acid (AA), respectively. The oxidation peaks for guanine and adenine at 0.628 V and 0.932 V can be clearly observed. The rates of the changes on the current densities of guanine (red column) and adenine (blue column) in the absence and in the presence of the interferents are presented in Fig. 5B. The change on the current densities of guanine and adenine was within 7.3%, showing the high tolerance from the potential interfering biomolecules that are presented in practical conditions. In the presence of the interferents, a simultaneous detection of guanine and adenine at the $Au_{50}Pt_{50}$NCs-rGO/GCE in a concentration range from 5.0 to 30 μM was examined (Fig. 5C). The peak current densities of guanine and adenine were gradually increased with the increase of the concentrations of guanine and adenine. Based on the peak current densities, the highly linear responses for guanine and adenine were observed (Fig. 5D). The presence of interferents had some but not significant interference towards the simultaneous detection of guanine and adenine; overall, the developed sensor exhibited satisfactory anti-interference ability. Figure 6 shows the repetitive measurements on the guanine and adenine with the $Au_{50}Pt_{50}$NCs-rGO/GCE, which was realized by

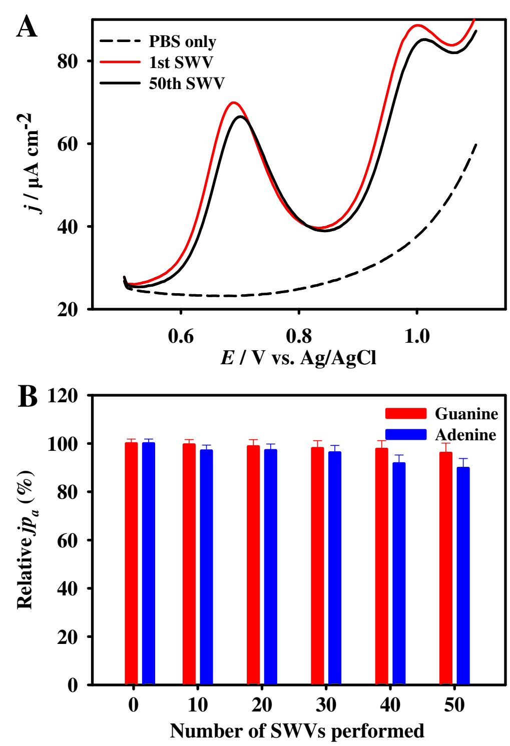

Fig. 6 (A) The 1st and 50th SWV responses of 50 μM guanine and adenine at the $Au_{50}Pt_{50}$NCs-rGO/GCE in 0.1 M PB (pH 7.2) solution. (B) The change in the current densities of guanine and adenine after various number of the repetitive measurements

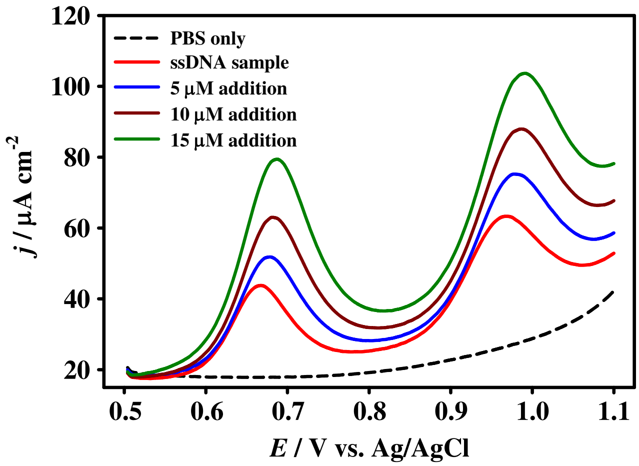

Fig. 7 SWV responses of the $Au_{50}Pt_{50}$NCs-rGO/GCE for the detection of guanine and adenine in salmon sperm DNA sample

continuously oxidizing 50 μM of guanine and adenine using SWV. In comparison with the 1st SWV curve of guanine and adenine oxidation at the $Au_{50}Pt_{50}$NCs-rGO/GCE, the oxidation potentials of guanine and adenine with the 50th SWV curve were only slightly shifted by 11 mV and 10 mV, respectively. The corresponding current densities were decreased by ca. 3.9% and 9.9% for guanine and adenine, respectively. These results demonstrated that the $Au_{50}Pt_{50}$NCs-rGO nanocomposite exhibited good stability under repeated measurements.

Real sample analysis To evaluate the practicality of the $Au_{50}Pt_{50}$NCs-rGO/GCE, salmon sperm ssDNA sample was prepared using thermal denaturation and examined using the prepared electrochemical sensor. Firstly, 50 μL of the ssDNA sample was added to the 10 mL PB solution (pH 7.2), and the SWV responses of guanine and adenine were recorded. Figure 7 shows the two distinct oxidation peaks of guanine and adenine at 0.660 V and 0.968 V, respectively, revealing the anti-interfering capability of the $Au_{50}Pt_{50}$NCs-rGO/GCE towards guanine and adenine in the presence of other biomolecules such as thymine and cytosine in real sample. The concentrations of guanine and adenine in the DNA sample were estimated by comparing the peak current densities with the calibration curves plotted previously in the simultaneous detection experiment. From the calibration curves, the concentrations of guanine and adenine in the salmon sperm DNA sample were estimated to be 12.5 ± 0.05 μM and 16.5 ± 0.04 μM, respectively. Furthermore, a ratio on (G+C):(A+T) was evaluated as 0.76, which was very close to the literature value of 0.77. Following the addition of the ssDNA sample, guanine and adenine in the standard solution with different concentrations (5.0, 10.0, 15.0 μM) were added. The current responses were recorded, and the recovery percentage was calculated (Table 1). The recovery percentages were well satisfied, between 92.8 and 102%. The results indicated the proposed electrochemical sensor fabricated in such a facile approach is a promising platform for the simultaneous detection of guanine and adenine and demonstrated its advantage of simplicity and rapidity over traditional analytical techniques such as HPLC and electrophoresis. However, incorporation of the fabricated electrode into a sensing device for further tests is needed for practical applications.

Conclusions

In summary, we have demonstrated a facile approach for the fabrication of the AuPtNCs-rGO/GCE nanocomposite for the simultaneous detection of guanine and adenine. The Au:Pt ratio in the as-synthesized nanocomposite was optimized to be 50:50 and the nanocomposite exhibited the excellent electrocatalytic activity towards the oxidation of guanine and adenine. The developed sensor showed the low detection limits of 60 nM and 100 nM for guanine and adenine, respectively. An extensive linear range from 1.0 μM to 0.20 mM was obtained for both biomolecules. Furthermore, the electrochemical sensor exhibited a high anti-interfering capability towards the detection of guanine and adenine in the presence of biomolecules such as ascorbic acid and dopamine, as well as a high stability. In comparison with SWV responses of the AuNCs-rGO/GCE and PtNCs-rGO/GCE, a synergistic effect was observed for the $AuPt_{50}Pt_{50}$NCs-rGO/GCE towards the electrochemical oxidation of guanine and adenine. The fabricated $Au_{50}Pt_{50}$NC-rGO nanocomposite was further applied to detect guanine and adenine in salmon sperm ssDNA sample to

Table 1 Determination of guanine and adenine in Salmon Sperm DNA, and recovery percentages using multiple additions of 5 μM guanine and adenine

Sample	Purine	Detected (μM)	Added (μM)	Found (μM)	Recovery %
Salmon sperm DNA	G	12.5	5	17.7	101
	G	12.5	10	22.9	102
	G	12.5	15	28.0	102
	A	16.5	5	21.0	97.7
	A	16.5	10	24.6	92.8
	A	16.5	15	29.0	92.1

evaluate its practicality in real sample application, and a satisfactory G+C/A+T ratio and recovery percentages were obtained. More importantly, the present work not only provided a simple synthetic method for graphene-supported bimetallic nanocluster nanocomposite, but also explored the possibility of using this synthetic approach to fabricate multi-metallic nanoclusters supported by rGO. It potentially opened an entrance of using these nanocomposites in industrial, environmental, and biomedical application.

Supplementary Information The online version contains supplementary material available at https://doi.org/10.1007/s00604-021-04926-7.

Funding This work was supported by a Discovery Grant from the Natural Sciences and Engineering Research Council of Canada (NSERC RGPIN-06248). A. Chen acknowledges NSERC and the Canada Foundation for Innovation (CFI) for the Canada Research Chair Award in Materials and Environmental Chemistry.

Declarations

Conflict of interest The authors declare no competing interests.

References

1. Hofer H, Liu Z, Balasubramanian S (2019) Detection, structure and function of modified DNA bases. J Am Chem Soc 141:6420–6429
2. Lord J, Ashworth A (2012) The DNA damage response and cancer therapy. Nature 481:287–294
3. Zeman K, Cimprich A (2014) Causes and consequences of replication stress. Nat Cell Biol 16:2–9
4. Yari A, Derki S (2016) New MWCNT-Fe_3O_4@PDA-Ag nanocomposite as a novel sensing element of an electrochemical sensor for determination of guanine and adenine contents of DNA. Sensors Actuators B Chem 227:456–466
5. Yan Z, Zhang D, Peng Q, Zheng L (2017) Colorimetric detection of DNA by using target catalyzed DNA nanostructure assembly and unmodified gold nanoparticles. Microchim Acta 184:4809–4815
6. Yu Q, Zhang J, Qiu W, Li K, Qian L, Zhang X, Liu G (2021) Gold nanorods-based lateral flow biosensors for sensitive detection of nucleic acids. Microchim Acta 188:133
7. Qi T, Song C, He J, Chen W, Kong D, Shi H, Tan L, Pan R, Tang S, Lee K (2020) Highly sensitive detection of multiple microRNAs by high-performance liquid chromatography coupled with long and short probe-based recycling amplification. Anal Chem 92:5033–5040
8. Carrillo-Carrión C, Armenta S, Simonet M, Valcárcel M, Lendl B (2011) Determination of pyrimidine and purine bases by reversed-phase capillary liquid chromatography with at-line surface-enhanced Raman spectroscopic detection employing a novel SERS substrate based on ZnS/CdSe silver–quantum dots. Anal Chem 83: 9391–9398
9. Chen A, Chatterjee S (2013) Nanomaterials based electrochemical sensors for biomedical applications. Chem Soc Rev 42:5425–5438
10. Chen A, Shah B (2013) Electrochemical sensing and biosensing based on square wave voltammetry. Anal Methods 5:2158–2173
11. Rahn L, Anand K (2021) Recent advancements in bipolar electrochemical methods of analysis. Anal Chem 93:103–123
12. Wang Y, Huang T, Liu J, Guo X, Abudukeyoumu G, Zhang Y, Ye C, Li C (2018) A novel electrochemical sensor based on Cu@Ni/MWCNTs nanocomposite for simultaneous determination of guanine and adenine. Biosens Bioelectron 102:389–395
13. Akturk M, Karabiberoglu U, Dursun Z (2018) Fabrication of Cu $-CeO_2$ coated multiwall carbon nanotube composite electrode for simultaneous determination of guanine and adenine. Electroanal 30:238–249
14. Chen A, Holt-Hindle P (2010) Platinum-based nanostructured materials: synthesis, properties, and applications. Chem Rev 110: 3767–3804
15. Pradhan S, Biswas S, Das K, Bhar R, Bandyopadhyay R, Pramanik P (2018) An efficient electrode for simultaneous determination of guanine and adenine using nano-sized lead telluride with graphene. New J Chem 42:564–573
16. He S, He P, Zhang X, Zhang X, Liu K, Jia L, Dong F (2018) Poly (glycine)/graphene oxide modified glassy carbon electrode: preparation, characterization and simultaneous electrochemical determination of dopamine, uric acid, guanine and adenine. Anal Chim Acta 1031:75–82
17. Abbaspour A, Mehrgardi M (2004) Electrocatalytic oxidation of guanine and DNA on a carbon paste electrode modified by cobalt hexacyanoferrate films. Anal Chem 76:5690–5696
18. Liu T, Zhu X, Cui L, Ju P, Qu X, Ai S (2011) Simultaneous determination of adenine and guanine utilizing PbO_2-carbon nanotubes-ionic liquid composite film modified glassy carbon electrode. J Electroanal Chem 651:216–221
19. Wang H, Zhang H, Jiang Y, Li X, Liu Y (2016) Determination of adenine and guanine by a dopamine-melanin nanosphere–polyaniline nanocomposite modified glassy carbon electrode. Anal Lett 49:226–235
20. Qian L, Thiruppathi AR, van der Zalm J, Chen A (2021) Graphene oxide-based nanomaterials for the electrochemical sensing of isoniazid. ACS Appl Nano Mater 4:3696–3706
21. Alam A, Deen M (2020) Bisphenol A electrochemical sensor using graphene oxide and β-cyclodextrin-functionalized multi-walled carbon nanotubes. Anal Chem 92:5532–5539
22. Qian L, Durairaj S, Prins S, Chen A (2021) Nanomaterial-based electrochemical sensors and biosensors for the detection of pharmaceutical compounds. Biosens Bioelectron 175:112836
23. Gao Y, Xu J, Lu L, Wu L, Zhang K, Nie T, Zhu X, Wu Y (2014) Overoxidized polypyrrole/graphene nanocomposite with good electrochemical performance as novel electrode material for the detection of adenine and guanine. Biosens Bioelectron 62:261–267
24. Arvand M, Ghodsi N, Zanjanchi M (2016) Nanomaterial-based electrochemical sensors and biosensors for the detection of pharmaceutical compounds. Biosens Bioelectron 77:837–844
25. Dubuisson E, Yang Z, Loh K (2011) Optimizing label-free DNA electrical detection on graphene platform. Anal Chem 83:2452–2460
26. Tian H, Wang L, Sofer Z, Pumera M, Bonanni A (2016) Doped graphene for DNA analysis: the electrochemical signal is strongly influenced by the kind of dopant and the nucleobase structure. Sci Rep 6:33046
27. Tao Y, Li M, Ren J, Qu X (2015) Metal nanoclusters: novel probes for diagnostic and therapeutic applications. Chem Soc Rev 44: 8636–8663
28. Lu Y, Chen W (2012) Sub-nanometre sized metal clusters: from synthetic challenges to the unique property discoveries. Chem Soc Rev 41:3594–3623
29. Liu Z, Nemec-Bakk A, Khaper N, Chen A (2017) Sensitive electrochemical detection of nitric oxide release from cardiac and cancer cells via a hierarchical nanoporous gold microelectrode. Anal Chem 89:8036–8043

30. Yang M, Chen X, Jiang T, Guo Z, Liu J, Huang X (2016) Electrochemical detection of trace arsenic(III) by nanocomposite of nanorod-like α-MnO_2 decorated with ~5 nm Au nanoparticles: considering the change of arsenic speciation. Anal Chem 88:9720–9728
31. Yahia-Ammar A, Sierra D, Mérola F, Hildebrandt N, Le Guével X (2016) Self-assembled gold nanoclusters for bright fluorescence imaging and enhanced drug delivery. ACS Nano 10:2591–2599
32. Pyo K, Thanthirig V, Kwak K, Pandurangan P, Ramakrishna G, Leem D (2015) Ultrabright luminescence from gold nanoclusters: rigidifying the Au(I)–thiolate Shell. J Am Chem Soc 137:8244–8250
33. Roy S, Baral A, Bhattacharjee R, Jana B, Datta A, Ghosh S, Banerjee A (2015) Preparation of multi-coloured different sized fluorescent gold clusters from blue to NIR, structural analysis of the blue emitting Au7 cluster, and cell-imaging by the NIR gold cluster. Nanoscale 7:1912–1920
34. Biltek S, Sen A, Pedicini A, Reber C, Khanna S (2014) Isolation and structural characterization of a silver–platinum nanocluster, $Ag_4Pt_2(DMSA)_4$. J Phys Chem A 118:8314–8319
35. Tiwari J, Nath K, Kumar S, Tiwari N, Kemp K, Le N, Youn D, Lee J, Kim K (2013) Stable platinum nanoclusters on genomic DNA-graphene oxide with a high oxygen reduction reaction activity. Nat Commun 4:2221
36. Le Guével X, Trouillet V, Spies C, Jung G, Schneider M (2012) Synthesis of yellow-emitting platinum nanoclusters by ligand etching. J Phys Chem C 116:6047–6051
37. Yang C, Shi K, Dou B, Xiang Y, Chai Y, Yuan R (2015) In situ DNA-templated synthesis of silver nanoclusters for ultrasensitive and label-free electrochemical detection of MicroRNA. ACS Appl Mater Interfaces 7:1188–1193
38. Mutharani B, Ranganathan P, Chen T, Chen S, Kumar J (2020) Thermoreversible switchlike electrocatalytic reduction of tizanidine based on a graphene oxide tethered stimuli-responsive smart surface supported Pd catalyst. Anal Chem 92:8965–8973
39. Govindhan M, Amiri M, Chen A (2015) Au nanoparticle/graphene nanocomposite as a platform for the sensitive detection of NADH in human urine. Biosens Bioelectron 66:474–480
40. Pal S, Chakraborty M, Sarkar N (2020) Graphene oxide functionalized with 5-aminophenanthroline for selective detection of adenine through fluorescence “Turn-Off-On” response. ACS Appl Nano Mater 4:3532–3539
41. Barua S, Dutta H, Gogoi S, Devi R, Khan R (2018) Nanostructured MoS_2-based advanced biosensors: a review. ACS Appl Nano Mater 1:2–25
42. Schaaff T, Knight G, Shafigullin M, Borkman R, Whetten R (1998) Isolation and selected properties of a 10.4 kDa gold:glutathione cluster compound. J Phys Chem B 102:10643–10646
43. Wanjala B, Luo J, Fang B, Mott D, Zhong C (2011) Gold-platinum nanoparticles: alloying and phase segregation. J Mater Chem 21:4012–4020
44. Qian L, Thiruppathi AR, Elmahdy R, van der Zalm J, Chen A (2020) Graphene-oxide-based electrochemical sensors for the sensitive detection of pharmaceutical drug naproxen. Sensors 20:1252
45. Liu Z, Forsyth H, Khaper N, Chen A (2016) Sensitive electrochemical detection of nitric oxide based on AuPt and reduced graphene oxide nanocomposites. Analyst 141:4074–4083
46. Suntivich J, Xu Z, Carlton C, Kim J, Han B, Lee W, Bonnet N, Marzari N, Allard L, Gasteiger H, Hamad-Schifferli K, Shao-Horn Y (2013) Surface composition tuning of au–Pt bimetallic nanoparticles for enhanced carbon monoxide and methanol electro-oxidation. J Am Chem Soc 135:7985–7991
47. Pruneanu S, Biris AR, Pogacean F, Coroş M, Kannarpady G, Watanabe F, Biris A (2014) The study of adenine and guanine electrochemical oxidation using electrodes modified with graphene-platinum nanoparticles composites. Electrochim Acta 139:386–393

Publisher's note Springer Nature remains neutral with regard to jurisdictional claims in published maps and institutional affiliations.